Atmos. Chem. Phys. Discuss., 11, 20245–20265, 2011
www.atmos-chem-phys-discuss.net/11/20245/2011/
doi:10.5194/acpd-11-20245-2011

Atmospheric Chemistry and Physics Discussions

Effects of model spatial resolution on the interpretation of satellite NO_2 observations

L. C. Valin[1], A. R. Russell[1], R. C. Hudman[1], and R. C. Cohen[1,2]

[1]College of Chemistry, University of California Berkeley, Berkeley, CA 94720, USA
[2]Department of Earth and Planetary Sciences, University of California Berkeley, Berkeley, CA 94720, USA

Received: 11 May 2011 – Accepted: 22 June 2011 – Published: 18 July 2011

Correspondence to: R. C. Cohen (rccohen@berkeley.edu)

Published by Copernicus Publications on behalf of the European Geosciences Union.

Abstract

Prediction of ozone production, a photochemically non-linear process, is known to be biased in coarse-resolution chemical transport models (CTM). Other species subject to non-linear sources or sinks are also susceptible. Here we compute the resolution-dependent bias in predicted NO_2 column, a quantity relevant to the interpretation of space-based observations. We use 1-D and 2-D models to illustrate the mechanisms responsible for these biases over a range of NO_2 concentrations and model resolutions. We find that the behavior of calculated biases in NO_2 depends on the magnitude and spatial extent of the NO_2 source. We use WRF-CHEM to determine the resolution necessary to predict column NO_2 to 10 % and 25 % over the Four Corners power plants in NW New Mexico, Los Angeles, and the San Joaquin Valley in California.

1 Introduction

NO_x ($NO + NO_2$) is emitted to the troposphere by fossil-fuel combustion, biomass burning, soil microbial processes, and lightning. In the troposphere, NO_x effects ozone production, aerosol formation and atmospheric composition (e.g. CH_4) through feedback on OH radical. The concentration of OH radical, the main daytime sink of NO_x, depends strongly on NO_x concentration. As a result, the removal rate of NO_x (i.e. $k_{NO_2+OH}[OH]$) depends strongly on its own concentration. To accurately quantify OH and NO_x lifetime, a model must accurately resolve NO_x concentrations from a source (100s ppb) to the background (100s ppt). Column NO_2 observations show that this transition can occur at scales as small as 10–20 km (Heue et al., 2008; Valin et al., 2011)

High quality satellite-based observations of tropospheric NO_2 have provided unique insights into spatial and temporal patterns on regional scales (e.g., Bertram et al., 2005; Beirle et al., 2010; Hudman et al., 2010; Russell et al., 2010; Mebust et al., 2011). These satellite observations have also provided constraints on inverse models

ACPD
11, 20245–20265, 2011

that are used to validate emission inventories (e.g., Martin et al., 2003; Kim et al., 2006; Konovalov et al., 2006; Toenges-Schuller et al., 2006; Napelenok et al., 2008). Most of the inverse modeling studies used to validate these emission inventories adjust NO_x emissions with the assumption that model chemistry is accurate. However, errors in our understanding of atmospheric reactions (e.g., Thornton et al., 2002; Mollner et al., 2010) or their representation in models may compromise the accuracy of these inferred emissions. For example, extensive research has demonstrated that modeled ozone production depends strongly on model resolution, a result of its nonlinear dependence on NO_x concentration (e.g., Sillman et al., 1990; Kumar et al., 1994; Gillani et al., 1996; Wild and Prather, 2006). This research suggests that OH, which has the same NO_x-dependence as ozone production, will also vary with model resolution affecting NO_2 lifetime and concentration. As a result, NO_x emissions derived from an inversion of satellite NO_2 observations may have resolution-dependent biases.

We investigate the dependence of predicted NO_2 on horizontal resolution in a 1-D plume model, a 2-D plume model, and in WRF-CHEM, a fully-coupled regional 3-D chemical transport model (CTM). We use the simpler models to understand the source of resolution-dependent biases and use WRF-CHEM to determine the model resolution necessary to predict column NO_2 to 10 % and 25 % accuracy over the Four Corners and San Juan power plants, the city of Los Angeles, and on a regional scale over the San Joaquin Valley in California.

2 NO_x-OH chemistry in a 1-D plume model

To begin the discussion, we simulate NO_2 outflow from a point source in one dimension. In this model, NO_2 is emitted at the western end of the domain (x = 0–1024 km) and transported to the east at a constant rate (5 m/s). We run the model with emission rates of 30, 3.0, and 0.30 kmol h^{-1} at resolutions of 0.5 to 512 km. The dimensions perpendicular to the flow are fixed at 1 km and is removed by OH. The concentration of OH is determined by an analytical solution

ACPD
11, 20245–20265, 2011

to the steady-state relationship of OH and NO_2 concentration, volatile organic reactivity ($k_{OH+VOC}[VOC] = 1\,s^{-1}$), HO_x production rate (0.5×10^7 molecules $cm^{-3}\,s^{-1}$), radical chain propagation rate ($k_{NO+RO_2 \rightarrow RO+NO_2} = 8 \times 10^{-12}$ molecules $cm^{-3}\,s^{-1}$) radical termination rates ($k_{RO_2+RO_2-Effective} = 7.5 \times 10^{-12}$ molecules $cm^{-3}\,s^{-1}$; $k_{NO_2+OH} = 9.3 \times 10^{-12}$ molecules $cm^{-3}\,s^{-1}$; $k_{NO+RO_2 \rightarrow RNO_3} = 0$ molecules $cm^{-3}\,s^{-1}$), and a ratio of NO_2 to NO_x (0.7) (Murphy et al., 2006).

Figure 1 shows the relationship of OH and NO_2 derived from this steady-state model and the corresponding NO_2 lifetime. As is well-known, the response of OH to changes in NO_2 depends on NO_2 concentration. For example, decreasing NO_2 results in an increase of OH and a shorter NO_2 lifetime at high NO_2 (red) while resulting in less OH and a longer NO_2 lifetime at low NO_2 (blue).

When 1-D simulations of large, intermediate, and small sources are run to steady-state, NO_2 is removed by OH such that the spatial gradient reflects the applied NO_2-OH feedback (Fig. 2). Failure to accurately resolve NO_2 results in inaccurate OH and biases in both the NO_2 lifetime and concentration. For example, when a large source of NO_2 is computed at 2 km resolution, OH is suppressed so strongly that NO_2 decays by only one e-fold in about 400 km (Fig. 2a,d – solid line). Computed at coarser resolution (128 km), NO_2 is numerically diluted such that OH is enhanced, NO_2 is shorter-lived, and NO_2 concentrations are biased low over the entire domain (Fig. 2a,d – dashed line). At this high emission rate, biases in the domain-total NO_2 exceed 50 % at the coarsest resolutions (Fig. 3, red line).

In contrast to a large source, NO_2 emitted from a small source decays rapidly when computed at 2 km resolution, a reflection of high OH concentration (Fig. 2c,f – solid line), but at coarser model resolution (128 km), the numerical dilution of NO_2 results in lower OH, a longer NO_2 lifetime, and a corresponding positive bias in NO_2 concentration (Fig. 2c,f – dashed line, Fig. 3, blue line).

For an intermediate source of NO_2, the plume decays by an e-fold within 60 km at 2 km model resolution, corresponding to a chemical lifetime of about three hours and maximum OH (Fig. 2b,e – solid line). Model calculations at coarser resolutions

ACPD
11, 20245–20265, 2011

(128 km) are not capable of resolving this sharp gradient. Because NO_2 concentrations predicted for an intermediate source are near the NO_2-OH crossover regime, biases behave like those of a large source at finer model resolutions and like those of a small source at coarser resolutions (Fig. 3, green line).

In a 1-D model, biases are less than 15 % at model resolutions finer than 128 km and are only large (>50 %) for the highest emission scenario (red) at the coarsest model resolution (Fig. 3).

3 Biases in a 2-D plume model

In a 2-D model we define a point source ($2 \times 2\,km^2$) with emission rates of 300, 30, and $3\,kmol\,h^{-1}$ and an area source ($96 \times 96\,km^2$) with emission rates of 1200, 120, and $12\,kmol\,h^{-1}$ both located in the far southwest corner ($x = y = 0$ km) of the domain ($x = y = 0$–384 km). These emission rates are selected so that the simulated plume concentration corresponds with the high, intermediate and low NO_2-OH feedback regimes depicted in Fig. 1. In this model, NO_2 is transported with x and y wind speeds of $3\,m\,s^{-1}$, a mean flow of $3\sqrt{2}\,m\,s^{-1}$ to the northeast. Diffusion rates are set to $10\,m^2\,s^{-1}$. Initial and boundary concentrations are set to 0.5 ppt. The model is computed at six grid resolutions (2, 4, 12, 24, 48, and 96 km), with layer height fixed at 1 km. We run simulations of NO_2 with OH determined by the steady state equation and with OH set constant at 5.5×10^6 molecules cm^{-3}

In two dimensions, a large source of NO_2 is OH-suppressing and long-lived when simulated at 2 km (Fig. 4a) but is OH-enhancing and short-lived when simulated at coarser resolutions (24 km, 96 km). As a result, predicted NO_2 is biased −75 % at 96 km resolution (Fig. 5b). Over a small source (not shown), the opposite effect is predicted. A small source is OH-enhancing and short-lived at 2 km resolution, but becomes OH-limiting and longer-lived at 96 km resolution. As a result, NO_2 predicted over a small source is biased 100 % high at 96 km resolution (Fig. 5b).

ACPD
11, 20245–20265, 2011

Figure 5 summarizes biases predicted in a 2-D model as a function of model resolution, source strength, and proximity to the source. Biases predicted for NO_2 in a constant OH field, that is one without feedback and only subject to transport effects (Fig. 5b–e, black line), are negligible over the entire domain (∼ 0 %, 5b), significant over the 192 km nearest the source (−10 %, 5c), and large in both the 96 km nearest the source (−30 %, 5d) and in a $12 \times 12\,km^2$ pixel 96 km downwind from the source (−75 %, 5e). When subjected to NO_2-OH chemical feedbacks (Fig. 5b–e, red, green, and blue lines), biases diverge from that of transport alone (black) with behavior depending, as expected, on the rate of NO_x emissions. Over each spatial domain considered, simulation of a large source (red) is biased low versus transport alone (black) whereas the opposite is true for a small source (blue). For both large and small sources, the magnitude of the bias increases as the model resolution coarsens.

For an area source (not shown), biases predicted follow the same pattern as those shown for a point source (Fig. 5) but are much smaller at all model resolutions (∼ 25 % at 96 km model resolution). The biases predicted for an area source are smaller because the source is already diluted ($96 \times 96\,km^2$).

Using a 2-D steady-state plume model with steady-state NO_2-OH feedbacks we show that biases in predicted NO_2 grow with coarsening resolution. The behavior of these biases depends on both the magnitude and spatial extent of the source. For this 2-D model, biases are predicted to be unacceptably large (∼ 75 %) at relevant horizontal resolutions (96 km) with behavior that depends dramatically on source strength (+100 % for small source to −75 % for large source) and source distribution (∼ 75 % for point source to ∼ 25 % for area source).

4 WRF-CHEM: Resolution required to predict column NO_2 to 10 % and 25 %

Air quality control strategies often use 10 or 25 % NO_x reductions as a realistic regulatory benchmark. Using WRF-CHEM (Grell et al., 2005), a state-of-the-art multi-scale regional 3-D air quality CTM, we examine the grid resolution necessary to attain 10 %

ACPD
11, 20245–20265, 2011

and 25 % accuracy for prediction of column NO_2 as would be observed by a satellite-based instrument such as OMI, SCIAMACHY or GOME-2 (Callies et al., 2000; Richter et al., 2005; Bucsela et al., 2006; Boersma et al., 2007; Celarier et al., 2008).

We simulate column NO_2 over the Four Corners and San Juan Power Plants in Northwest New Mexico at 1, 4, 12, and 24 km resolution. We then simulate column NO_2 over California at 4, 12, 24, 48, and 96 km resolution. For a more detailed description of the WRF-CHEM simulations see the Appendix.

Like the steady-state NO_2-OH mechanism used in the plume models, WRF-CHEM predicts that OH depends non-linearly on NO_2 concentration (Fig. 6). For instance in a 1 km resolution simulation of Four Corners, simulated OH is low ($<5 \times 10^6$ molecules cm^{-2}) where NO_2 concentration is high (6a, red), enhanced ($>1.5 \times 10^7$ molecules cm^{-3}) where NO_2 is intermediate (6a, green) and low ($\sim 5 \times 10^6$ molecules cm^{-3}) where NO_2 is low (6a, blue). Since NO_2-OH feedbacks in WRF behave as those in the steady state model, WRF-CHEM predictions of NO_2 should be biased low at coarser model resolutions. Indeed, NO_2 column is biased −3 % at 4 km resolution, biased −27 % at 12 km resolution, and biased −50 % at 24 km resolution (Fig. 7). Relative to a 4 km simulation over Los Angeles, predicted NO_2 column is biased −7 % at 12 km resolution, −21 % at 48 km resolution, and −58 % at 96 km resolution (Fig. 8). Over the San Joaquin Valley, the biases are −16 % at 12 km resolution, −24 % at 24 km resolution and −36 % at 48 km resolution (Fig. 9).

Over Four Corners, Los Angeles, and the San Joaquin Valley, all regions of high NO_2 (Figs. 7–9), the size of the predicted bias depends on the spatial extent of the source. For example, 4 km resolution is sufficient to predict column NO_2 over the Four Corners power plants to better than 10 % (Fig. 7a–b) while 12 km model resolution is sufficient to achieve the same accuracy over Los Angeles (Fig. 8a–c).

ACPD
11, 20245–20265, 2011

5 Conclusions

We investigate the effects of NO_2-OH chemical feedbacks on predicted NO_2 in a 1-D plume model, a 2-D plume model, and WRF-CHEM, a fully-coupled 3-D CTM. We use 1-D and 2-D plume models to demonstrate that nonlinear NO_2-OH chemical feedback leads to biases in column NO_2 that depend on model resolution, source magnitude, and the spatial extent of the source. Any inference of NO_x emission inventories from chemical transport models will suffer biases that depend on the horizontal resolution of the model. Using WRF-CHEM, we determine the model resolution necessary to predict column NO_2 to 10 % and 25 % accuracy over Los Angeles, the San Joaquin Valley, and Four Corners. We find that prediction to 10 % accuracy requires model resolution of 4 km over both Four Corners and the San Joaquin Valley while 12 km is sufficient over Los Angeles.

Appendix A

We simulate column NO_2 from 1–7 July 2006, over California, Nevada, Northern Mexico, and the Eastern Pacific centered over Southern California ($2304 \times 2304\,km^2$) at 4, 12, 24, 48, and 96 km resolution. The simulated domain is much larger than the region of interest to ensure that there are no effects of boundary conditions in the coarser resolution model simulations. The first two days of simulation are used as spin-up, and the last five days (3–7 July) are averaged to 1 p.m. LST for all analyses. Emissions are the National Emission Inventory (NEI) 2005 onroad and offroad transportation emissions for a typical July weekday and Continuous Emissions Monitoring (CEMS) averaged point source emissions for a typical August, 2006, weekday. For more information, see ftp://aftp.fsl.noaa.gov/divisions/taq/emissions_data_2005/Weekday_emissions/readme.txt. Biogenic emissions for all model resolutions were generated by an online module as in (Grell et al., 2005) at 4 km horizontal resolution for a single July day and kept constant throughout the 7-day simulation. We use

ACPD
11, 20245–20265, 2011

the Regional Acid Deposition Model, version 2 chemical mechanism (Stockwell et al., 1990). The initial and boundary chemical conditions are derived from idealized profiles that are standard in WRF-CHEM. Radiative feedback from clouds on photolysis rates was disabled in order to simulate column NO_2 under clear-sky conditions that are typical of satellite observations. Meteorological initial and boundary conditions for the simulation are derived from the North American Regional Reanalysis for July 2005 (NARR – http://nomads.ncdc.noaa.gov/dods/NCEP_NARR_DAILY).

We simulate column NO_2 over the Four Corners region in the Western US ($384 \times 384\,km^2$) at 1, 4, and 12 km resolution and extend the boundaries ($1536 \times 1536\,km^2$) to simulate the same domain at 24 km resolution. This domain is centered on the Four Corners and San Juan Power Plants, which are approximately 20 km apart. This simulation is run in the same manner as that run over California except that only emissions from point sources are included. For simulation at 24 km resolution, as mentioned, the domain is extended to avoid boundary relaxation effects that occur over the 5 boundary grid cells in WRF-CHEM.

Acknowledgements. This work was supported by CARB under Grant #06-328, NASA under Grant #NNX08AE566, and by NASA Headquarters under the NASA Earth and Space Science Fellowship Program – Grant NESSF09.

References

Beirle, S., Huntrieser, H., and Wagner, T.: Direct satellite observation of lightning-produced NO_x, Atmos. Chem. Phys., 10, 10965–10986, doi:10.5194/acp-10-10965-2010, 2010.

Bertram, T. H., Heckel, A., Richter, A., Burrows, J. P., and Cohen, R. C.: Satellite measurements of daily variations in soil NO_x emissions, Geophys. Res. Lett., 32, L24812, doi:10.1029/2005GL024640, 2005.

Boersma, K. F., Eskes, H. J., Veefkind, J. P., Brinksma, E. J., van der A, R. J., Sneep, M., van den Oord, G. H. J., Levelt, P. F., Stammes, P., Gleason, J. F., and Bucsela, E. J.: Near-real time retrieval of tropospheric NO_2 from OMI, Atmos. Chem. Phys., 7, 2103–2118, doi:10.5194/acp-7-2103-2007, 2007.

ACPD
11, 20245–20265, 2011

Bucsela, E. J., Celarier, E. A., Wenig, M. O., Gleason, J. F., Veefkind, J. P., Boersma, K. F., and Brinksma, E. J.: Algorithm for NO_2 vertical column retrieval from the Ozone Monitoring Instrument, IEEE T. Geosci. Remote, 44, 1245–1258, doi:10.1109/tgrs.2005.863715, 2006.

Callies, J., Corpaccioli, E., Eisinger, M., Hahne, A., and Lefebvre, A.: GOME-2 – METOP's second-generation sensor for operational ozone monitoring, ESA Bull.-Eur. Space, 102, 28–36, 2000.

Celarier, E. A., Brinksma, E. J., Gleason, J. F., Veefkind, J. P., Cede, A., Herman, J. R., Ionov, D., Goutail, F., Pommereau, J. P., Lambert, J. C., van Roozendael, M., Pinardi, G., Wittrock, F., Schonhardt, A., Richter, A., Ibrahim, O. W., Wagner, T., Bojkov, B., Mount, G., Spinei, E., Chen, C. M., Pongetti, T. J., Sander, S. P., Bucsela, E. J., Wenig, M. O., Swart, D. P. J., Volten, H., Kroon, M., and Levelt, P. F.: Validation of ozone monitoring instrument nitrogen dioxide columns, J. Geophys. Res.-Atmos., 113, D15s15, doi:10.1029/2007jd008908, 2008.

Gillani, N. V., and Pleim, J. E.: Sub-grid-scale features of anthropogenic emissions of NO_x and VOC in the context of regional Eulerian models, Atmospheric Environment, 30, 2043-2059, doi:10.1016/1352-2310(95)00201-4,1996.

Grell, G. A., Peckham, S. E., Schmitz, R., McKeen, S. A., Frost, G., Skamarock, W. C., and Eder, B.: Fully coupled "online" chemistry within the WRF model, Atmos. Environ., 39, 6957–6975, 2005.

Heue, K.-P., Wagner, T., Broccardo, S. P., Walter, D., Piketh, S. J., Ross, K. E., Beirle, S., and Platt, U.: Direct observation of two dimensional trace gas distributions with an airborne Imaging DOAS instrument, Atmos. Chem. Phys., 8, 6707–6717, doi:10.5194/acp-8-6707-2008, 2008.

Hudman, R. C., Russell, A. R., Valin, L. C., and Cohen, R. C.: Interannual variability in soil nitric oxide emissions over the United States as viewed from space, Atmos. Chem. Phys., 10, 9943–9952, doi:10.5194/acp-10-9943-2010, 2010.

Kim, S. W., Heckel, A., McKeen, S. A., Frost, G. J., Hsie, E. Y., Trainer, M. K., Richter, A., Burrows, J. P., Peckham, S. E., and Grell, G. A.: Satellite-observed US power plant NO_x emission reductions and their impact on air quality, Geophys. Res. Lett., 33, 5, L22812, doi:10.1029/2006gl027749, 2006.

Konovalov, I. B., Beekmann, M., Richter, A., and Burrows, J. P.: Inverse modelling of the spatial distribution of NO_x emissions on a continental scale using satellite data, Atmos. Chem. Phys., 6, 1747–1770, doi:10.5194/acp-6-1747-2006, 2006.

Kumar, N., Odman, M. T., and Russell, A. G.: Multiscale air quality modeling: Application to

ACPD
11, 20245–20265, 2011

Southern California, J. Geophys. Res.-Atmos., 99, 5385–5397, 1994.
Martin, R. V., Jacob, D. J., Chance, K., Kurosu, T. P., Palmer, P. I., and Evans, M. J.: Global inventory of nitrogen oxide emissions constrained by space-based observations of NO_2 columns, J. Geophys. Res.-Atmos., 108, 4537, doi: 10.1029/2003JD003453, 2003.
Mebust, A. K., Russell, A. R., Hudman, R. C., Valin, L. C., and Cohen, R. C.: Characterization of wildfire NO_x emissions using MODIS fire radiative power and OMI tropospheric NO_2 columns, Atmos. Chem. Phys., 11, 5839-5851,doi:10.5194/acp-11-5839-2011, 2011
Mollner, A. K., Valluvadasan, S., Feng, L., Sprague, M. K., Okumura, M., Milligan, D. B., Bloss, W. J., Sander, S. P., Martien, P. T., Harley, R. A., McCoy, A. B., and Carter, W. P. L.: Rate of gas phase association of hydroxyl radical and nitrogen dioxide, Science, 330, 646–649, doi:10.1126/science.1193030, 2010.
Murphy, J. G., Day, D. A., Cleary, P. A., Wooldridge, P. J., Millet, D. B., Goldstein, A. H., and Cohen, R. C.: The weekend effect within and downwind of Sacramento: Part 2. Observational evidence for chemical and dynamical contributions, Atmos. Chem. Phys. Discuss., 6, 11971–12019, doi:10.5194/acpd-6-11971-2006, 2006.
Napelenok, S. L., Pinder, R. W., Gilliland, A. B., and Martin, R. V.: A method for evaluating spatially-resolved NO_x emissions using Kalman filter inversion, direct sensitivities, and space-based NO_2 observations, Atmos. Chem. Phys., 8, 5603–5614, doi:10.5194/acp-8-5603-2008, 2008.
Richter, A., Burrows, J. P., Nuss, H., Granier, C., and Niemeier, U.: Increase in tropospheric nitrogen dioxide over China observed from space, Nature, 437, 129–132, doi:10.1038/nature04092, 2005.
Russell, A. R., Valin, L. C., Bucsela, E. J., Wenig, M. O., and Cohen, R. C.: Space-based constraints on spatial and temporal patterns of NO_x emissions in California, 2005–2008, Environ. Sci. Technol., 44, 3608–3615, doi:10.1021/es903451j, 2010.
Sillman, S., Logan, J. A., and Wofsy, S. C.: A regional scale-model for ozone in the United States with subgrid representation of urban and power-plant plumes, J. Geophys. Res.-Atmos., 95, 5731–5748, 1990.
Stockwell, W. R., Middleton, P., Chang, J. S., and Tang, X. Y.: The 2nd generation Regional Acid Deposition Model chemical mechanism for regional air-quality modeling, J. Geophys. Res.-Atmos., 95, 16343–16367, 1990.
Thornton, J. A., Wooldridge, P. J., Cohen, R. C., Martinez, M., Harder, H., Brune, W. H., Williams, E. J., Roberts, J. M., Fehsenfeld, F. C., Hall, S. R., Shetter, R. E., Wert, B. P.,

ACPD
11, 20245–20265, 2011

and Fried, A.: Ozone production rates as a function of NO_x abundances and HO_x production rates in the Nashville urban plume, J. Geophys. Res.-Atmos., 107, 4146, doi:10.1029/2001jd000932, 2002.

Toenges-Schuller, N., Stein, O., Rohrer, F., Wahner, A., Richter, A., Burrows, J. P., Beirle, S., Wagner, T., Platt, U., and Elvidge, C. D.: Global distribution pattern of anthropogenic nitrogen oxide emissions: correlation analysis of satellite measurements and model calculations, J. Geophys. Res.-Atmos., 111, D05312, doi: 10.1029/2005JD006068, 2006.

Valin, L. C., Russell, A. R., Bucsela, E. J., Veefkind, J. P., and Cohen, R. C.: Observation of slant column NO_2 using the super-zoom mode of AURA-OMI, Atmos. Meas. Tech. Discuss., 4, 1989–2005, doi:10.5194/amtd-4-1989-2011, 2011.

Wild, O. and Prather, M. J.: Global tropospheric ozone modeling: quantifying errors due to grid resolution, J. Geophys. Res.-Atmos., 111, D11305, doi:10.1029/2005jd006605, 2006.

ACPD

11, 20245–20265, 2011

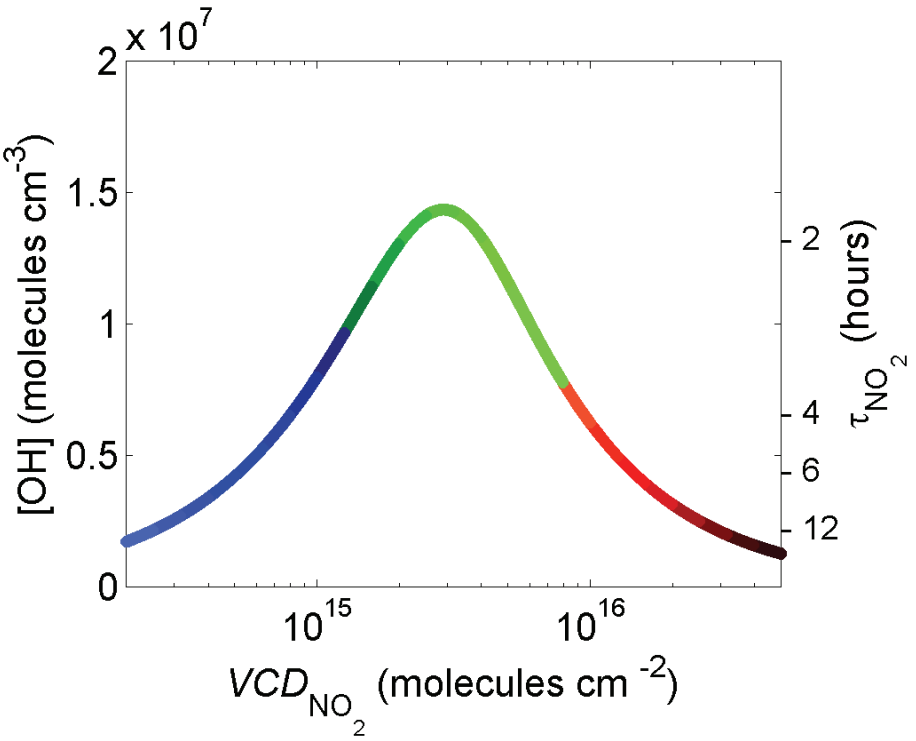

Fig. 1. Steady state OH concentration (left axis) and corresponding NO_2 lifetime ($1/k_{NO_2+OH} \times$ OH, right axis) versus boundary layer column NO_2 (molecules cm^{-2}) assuming a 1-km well-mixed boundary layer.

ACPD
11, 20245–20265, 2011

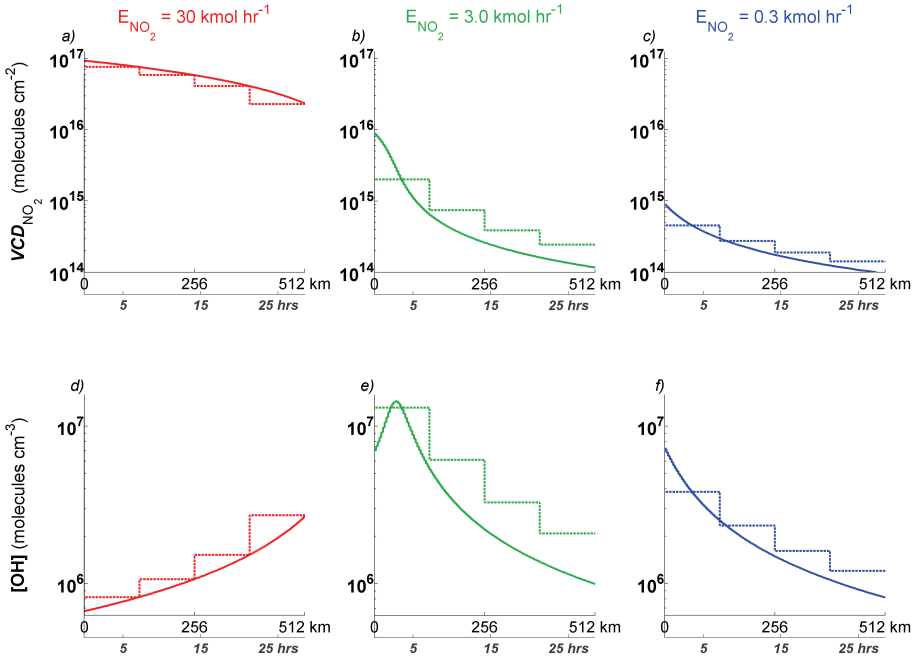

Fig. 2. Column NO_2 predicted in a 1-D plume model at 2 km (solid) and 128 km model resolutions (dashed) for **(a)** a large, **(b)** intermediate, and **(c)** small source of NO_2 and **(d–f)** the corresponding OH feedback. The color-scheme corresponds to NO_2-OH feedback regimes depicted in Fig. 1. Horizontal (N–S) and vertical layers are fixed at 1 km for all resolutions.

ACPD
11, 20245–20265, 2011

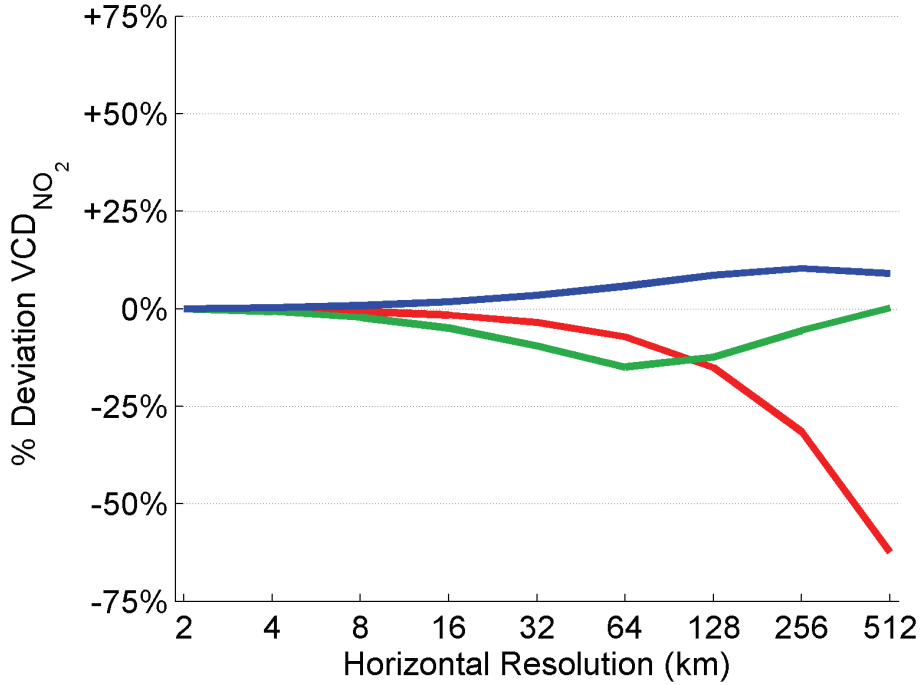

Fig. 3. Resolution-dependent bias in domain-averaged NO_2 concentration versus model resolution for small (blue), intermediate (green), and a large (red) sources of NO_2 in a 1-D plume model (Fig. 2).

ACPD
11, 20245–20265, 2011

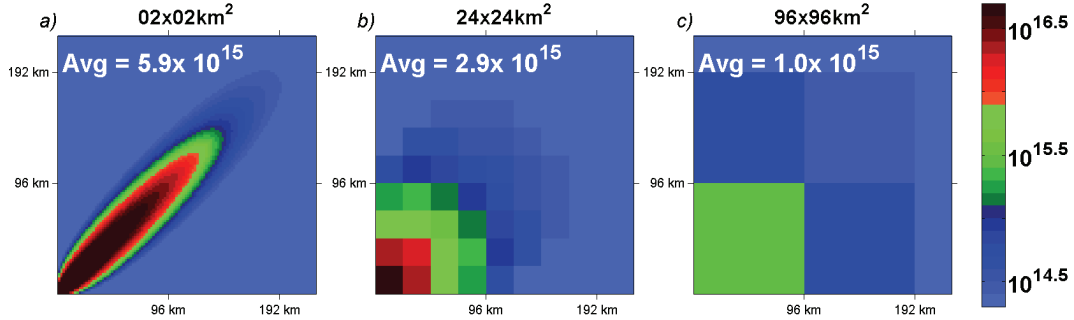

Fig. 4. Column NO_2 predicted in a 2-D plume model for a large point source simulated at **(a)** 2 km, **(b)** 24 km, and **(c)** 96 km resolution. The color-scheme corresponds to NO_2-OH feedback regimes depicted in Fig. 1. The vertical layer is fixed at 1 km for all simulations shown.

ACPD
11, 20245–20265, 2011

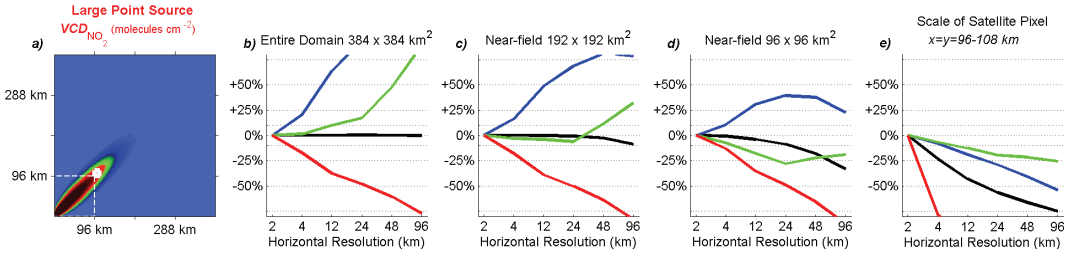

Fig. 5. **(a)** Column NO_2 predicted in a 2-D plume model for a large source simulated at 2 km resolution. Resolution-dependent bias in domain-averaged NO_2 concentration over the **(b)** entire domain ($x = y = 0$–384 km), **(c)** the 192 km near-field ($x = y = 0$–192 km), **(d)** the 96 km near-field ($x = y = 0$–96 km), and **(e)** at a point downwind ($x = y = 96$–108) for NO_2 emitted from a large (red), an intermediate (green), and a small (blue) point source of NO_2 with OH = f_{NO_2} as in Fig. 1 and from a large point source with OH set to 5×10^6 molecules cm^{-3} (black).

ACPD
11, 20245–20265, 2011

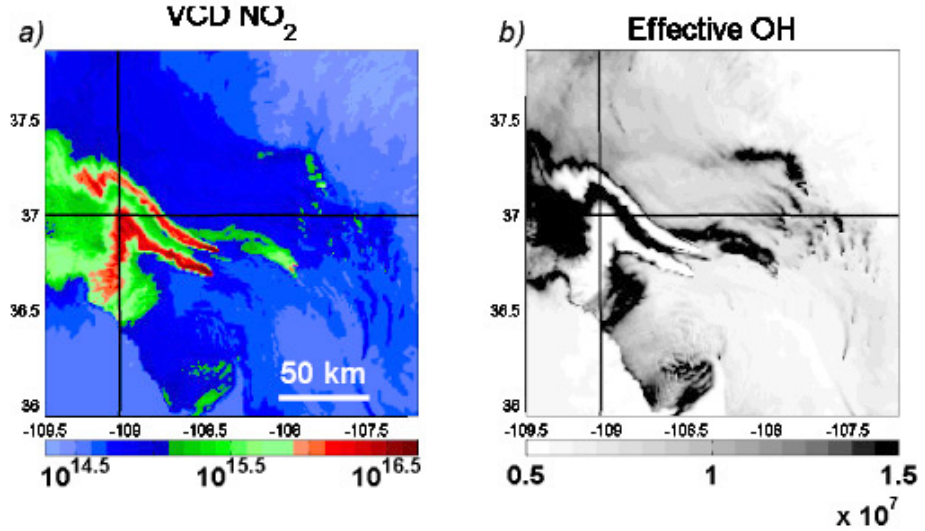

Fig. 6. (a) Column NO_2 (molecules cm^{-2}) and **(b)** effective OH (molecule cm^{-3}) simulated with WRF-CHEM at 1 km resolution over the Four Corners Region of US at 10 a.m. on 5 July 2006.

ACPD
11, 20245–20265, 2011

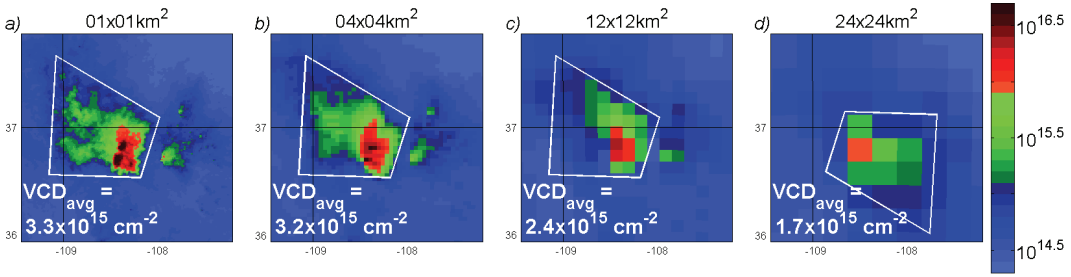

Fig. 7. WRF-CHEM 3–7 July 2006, 1 p.m. LST average column NO_2 (molecules cm^{-2}) simulated over Four Corners Region of US at **(a)** 1 km, **(b)** 4 km, **(c)** 12 km, and **(d)** 24 km model resolution. Column NO_2 is averaged over a sub-domain (white box) and reported in the bottom left corner of each panel. The sub-domain in the 24 km simulation was rotated to include the plume, which was predicted further to the SE than those predicted at 1, 4, or 12 km resolution.

ACPD
11, 20245–20265, 2011

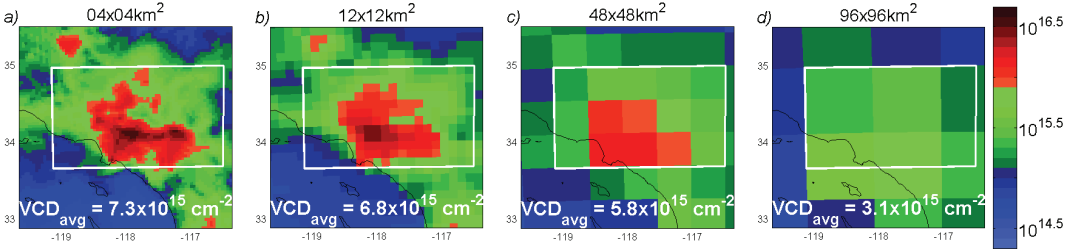

Fig. 8. WRF-CHEM 3–7 July 2006, 1 p.m. LST average column NO_2 (molecules cm^{-2}) simulated over Los Angeles at **(a)** 4 km, **(b)** 12 km, **(c)** 48 km, and **(d)** 96 km model resolution. Column NO_2 is averaged over a sub-domain (white box) and reported at the bottom of each panel.

ACPD
11, 20245–20265, 2011

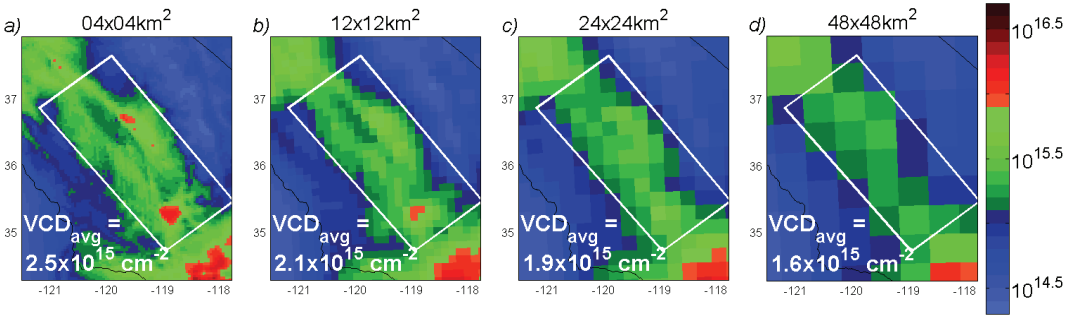

Fig. 9. WRF-CHEM 3–7 July 2006, 1 p.m. LST average column NO_2 (molecules cm^{-2}) over the San Joaquin Valley at **(a)** 4 km, **(b)** 12 km, **(c)** 24 km, and **(d)** 48 km model resolution. Column NO_2 is averaged over a sub-domain (white box) and reported at the bottom of each panel.

ACPD
11, 20245–20265, 2011